

Ultra-Fast Dual-Stage Vertical Positioning for High Performance SPMs

Andrew J. Fleming[†]

School of Electrical Eng. and Computer Science
The University of Newcastle
NSW 2300, Australia

Brian J. Kenton* and Kam K. Leang[‡]

Department of Mechanical Engineering
University of Nevada - Reno
Reno, NV 89557-0312 USA

Abstract—A major speed limitation of Scanning Probe Microscopes (SPMs) is the low vertical feedback bandwidth imposed by the mechanical scanner resonances. The vertical feedback controller regulates the tip-sample interaction in application modes such as constant-current scanning tunneling microscopy and constant-force atomic force microscopy. To increase the vertical feedback bandwidth, dual-stage actuators have been proposed to increase the first resonance frequency. In this work, an ultra-fast dual-stage vertical positioner and control system are described. The first resonance frequency of the dual-stage positioner is 88 kHz which permits a one-hundred fold speed increase of a commercial AFM. The dual-stage system is simple, low-cost and can be retrofitted to almost any commercial SPM.

I. INTRODUCTION

One of the foremost weaknesses of scanning probe microscopes is the slow speed at which images are recorded. Standard commercial microscopes scan at speeds of typically 1 to 10 lines per second, so a single image may take minutes to acquire. Although in many applications the slow imaging time is simply an inconvenience, in other applications, this becomes a critical limitation. Examples where speed is a primary concern include: large-range surface inspection [1], [2], nanofabrication [3]–[6], and imaging of fast biological and physical processes [7]–[12].

There are three main limitations to the speed of a scanning probe microscope. These are reviewed in reference [13] as: 1) the resonance frequency or bandwidth of the probe; 2) the bandwidth of the scanner and acquisition system; and 3) the bandwidth of the vertical feedback system. Extensive research has proceeded in recent years to reduce or eliminate these limitations. Recent reviews can be found in references [14]–[17].

Although major improvements have been made to the imaging speed of scanning probe microscopes, some of these techniques require highly specialized hardware, have low scan ranges, and require tiny sample sizes [9]–[12], [18], [19]. More moderate but still substantial speed increases have also been achieved by better control of existing hardware. Such techniques include: actuator linearization [20]–[22], feedforward control [22], input shaping [23], and improved feedback control [10], [18], [22], [24].

[†]Email: Andrew.Fleming@newcastle.edu.au, Voice: +61.2.4921.6493.

*Graduate student; [‡]Email: kam@unr.edu, Voice: +1.775.784.7782; Fax: +1.775.784.1701.

When the scanner performance of an SPM is improved, the major speed limitation becomes the vertical feedback bandwidth [10], [14], [15], [18]. In reference [13], the maximum vertical feedback bandwidth was shown to be the first resonance frequency divided by the peak amplitude, that is

$$\text{max. bandwidth} < \frac{\omega_1}{P},$$

where ω_1 is the first resonance frequency and P is the linear magnitude. For example, the scanner described in the following section has a resonance frequency of 680 Hz and a peak amplitude of 5.6 (15 dB). This implies a bandwidth limit of approximately 120 Hz. This is sufficient for a scan-rate of around 1 Hz or an imaging time of 100 seconds for a 100x100 resolution image. To increase the imaging rate to one frame per second, the vertical feedback bandwidth needs to be improved by two orders of magnitudes. That is, the resonance frequency and vertical feedback bandwidth need to be greater than 68 kHz and 12 kHz respectively, which is difficult with standard scanner designs.

Aside from the video-speed microscopes discussed above [8]–[12], techniques aimed at eliminating the scanner dynamics from the feedback loop include piezoelectric actuated probes [25], magnetically actuated probes [26], and electrostatically actuated probes [27]. Although such techniques can achieve significant improvements, they have not become wide spread as the probes and imaging modes are highly specialized and may not be compatible with standard microscopes.

Recently, dual-stage vertical positioning has been proposed for increasing the vertical feedback bandwidth [13], [16], [28], [29]. This technique involves an auxiliary positioning device with high resonance frequency used in a dual-stage configuration with the standard microscope positioner. The auxiliary system is low-cost, mechanically and electrically simple, and can be retrofitted to practically any scanning probe microscope.

In this work, the design of a high-speed dual-stage mechanism is described. The device consists of a small piezoelectric stack and flexure to restrain lateral modes. The first resonance frequency is predicted to be 88 kHz which allows a one-hundred-fold increase in the vertical feedback bandwidth and scan rate.

This paper begins in the following Section with a description of the microscope used in this work. A brief introduction



Fig. 1. The NT-MDT Ntegra scanning probe microscope arranged in scan-by-probe configuration. The scan head is mounted above a stationary sample platform.

to the dual-stage technique is then provided in Section III followed by a discussion of the mechanical design in IV. Imaging experiments and conclusions follow in Sections V and VI

II. EXPERIMENTAL SETUP

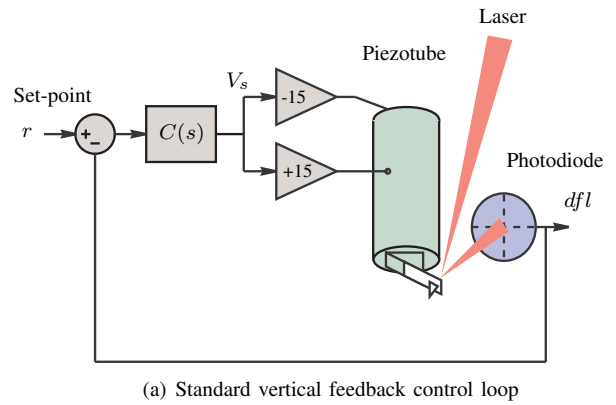
A. Microscope configuration

In this work, an NT-MDT Ntegra scanning probe microscope is used to demonstrate the proposed techniques. The scanner is an NT-MDT Z50309c1 piezoelectric tube scanner with 100- μm lateral range and 10- μm vertical range. The scanner comprises two piezoelectric tubes joined at the base. One tube is used for lateral positioning, and the other for vertical positioning. The internal and external electrodes of the vertical positioner are driven with equal but opposite voltages.

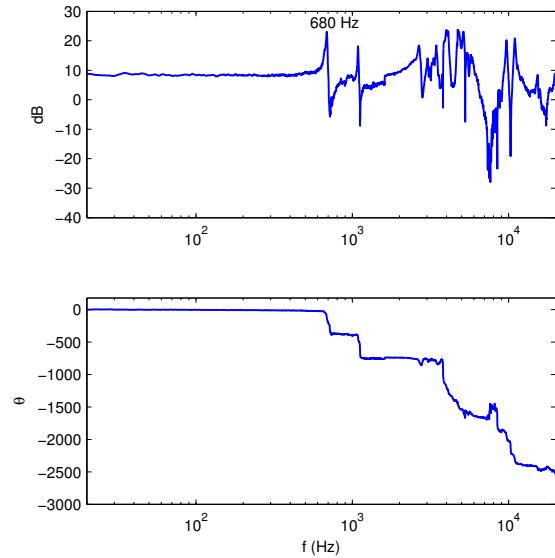
A signal access module allows direct access to the cantilever deflection, scanner electrode voltages, and reference trajectory. The cantilever is a TR800PSA Olympus Biolever with a resonance frequency of 73 kHz and a stiffness of 0.57 N/m.

B. Vertical Feedback Dynamics

The contact-mode vertical feedback system for an atomic force microscope is pictured in Figure 2(a). The piezoelectric tube scanner moves the probe in a vertical direction to regulate the cantilever deflection dfl to the set-point r . Although the diagram in Figure 2(a) represents an AFM operating in constant-force contact-mode, the schematic is similar to all forms of SPM where the tip-sample interaction is controlled. The only difference between operating modes is the measured feedback variable. For example, in contact-mode AFM, the feedback variable is cantilever deflection, while in STM, the feedback variable is tunneling current. Other feedback variables include the cantilever oscillation magnitude in tapping-mode AFM and the fiber oscillation magnitude in scanning near-field optical microscopy. All



(a) Standard vertical feedback control loop



(b) Frequency response of the standard vertical positioning system G_{dV_s} measured from the applied voltage V_s to the cantilever deflection dfl

Fig. 2. Schematic diagram (a) and frequency response (b) of a standard vertical feedback control system

of these modes share the same feedback system but with different feedback variables or methods of detection.

The microscope vertical feedback controller is an integral controller, i.e.,

$$C(s) = \frac{\alpha}{s} \quad (1)$$

Integral controllers are popular as they are simple to implement, provide good regulation of tip-sample interaction at low frequencies, and are easily adjustable. Ease of tuning is a necessity as the feedback system must accommodate many different SPM modes and cope with a wide range of probes and samples.

The frequency response from the control voltage V_s to the measured deflection dfl is plotted in 2(b). This includes the amplifier dynamics, the scanner and cantilever mechanics and the tip-sample interaction. This system is denoted G_{dV_s} , where

$$G_{dV_s}(s) = \frac{dfl(s)}{V_s}. \quad (2)$$

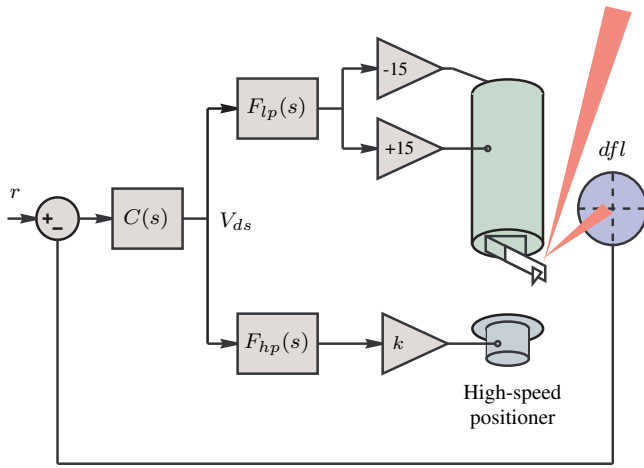


Fig. 3. Dual-stage diagram

The response is essentially flat from DC to 680 Hz where the first resonance frequency of the scanner occurs. This is the first lateral bending mode of the tube coupled into the vertical response [30].

Due to the resonance at 680 Hz, the vertical feedback bandwidth is limited to only 120 Hz. This reduces further to 68 Hz, if the controller gain is reduced to allow for a 6 dB gain-margin [13]. The imaging consequences of the low vertical feedback bandwidth are discussed in Section V.

III. DUAL-STAGE POSITIONING

To eliminate the low-frequency scanner resonances from the vertical feedback loop, a dual-stage vertical positioning system is illustrated in Figure 3. The auxiliary high-speed stage provides fast, short-range motions for imaging while the tube provides slower, long-range positioning for drift compensation and probe landing. The complementary high- and low-pass filters $F_{hp}(s)$ and $F_{lp}(s)$ combine the response of the two positioners so they appear as a single positioner with large range and high resonance frequency. The filter cut-off frequency is chosen to be approximately one tenth the resonance frequency of the tube scanner [13]. The gain k is chosen so that the sensitivity of the high- and low-frequency paths are equal.

Since the first resonance frequency in the control loop is now based only on the high-speed positioner, the vertical feedback bandwidth can be drastically increased. The design of a high-speed mechanical system is discussed in the following section.

Although the discussion thus far has focused on a scan-by-probe microscope, a high-speed positioner can also be added to a scan-by-sample microscope. In this configuration, the high-speed stage is attached either to the sample scanner or the stationary probe holder.

IV. MECHANICAL DESIGN

To obtain a high resonance frequency, the dual-stage positioner must be both stiff and light-weight. This can be accomplished with a small piezoelectric stack actuator. Two

TABLE I

SUMMARY OF CHARACTERISTIC VALUES FOR PIEZOACTUATORS.

Shape	Size (mm)	Range (μm)	Cap. (nF)	I (mm^4)	R_g (mm)	Res (kHz)
Plate	5×5×4	2.9	100	52	1.4	44
Ring	6×2×4	2.6	95	170	1.8	44

types of actuator were considered for the z -axis positioner: a 4 mm long ring-stack actuator with outside and inside diameters of 6 mm and 2 mm, respectively; and a 4 mm long, 5 mm by 5 mm plate-stack actuator. Table I compares their range, capacitance, second moment of inertia I , radius of gyration R_g , and dominant resonance when constrained at the base. Both actuators have approximately the same cross-sectional area and resonance frequency of 44 kHz.

The ring-stack actuator is preferable to the plate-stack actuator since it has a lower capacitance, higher second moment of inertia value I , and improved radius of gyration R_g . The circular cross-section of the ring-stack actuator is also compatible with an annular ring flexure that can be used to guide the motion of the free end, increase the dominant resonant frequency, and minimize out-of-axis vibration. The circular cross-section of the ring-stack actuator does not result in the concentrated flexure strains associated with the plate-stack actuator.

Finite element analysis was applied to investigate the dynamic behavior of two possible mounting configurations for the ring-stack: (1) base-constrained with a 1 mm thick sample mass (218 mg) and (2) base-constrained with the free end guided by an annular flexure. The actuator is a 4 mm long Noliac SCMAR01 ring stack. For the based-constrained case, the dominant mode at 40 kHz is an undesirable bending mode rather than a longitudinal mode as illustrated in Figure 4(b). The bending mode can cause significant distortion in AFM imaging.

To increase the resonance frequency of the bending mode, the second configuration employs a circular flexure to guide the free end [see Figures 4(d)-(f)]. The FEA results for this configuration show significant improvement in the mechanical resonance compared to the original, base-constrained case with no flexure [see Figures 4(a)-(c)]. Particularly, the bending modes (in x/y) occur above 90 kHz and the first vibration mode (piston mode) occurs at 88 kHz.

The mechanical assembly of the flexure-guided z -axis stage is pictured in Figure 5. This consists of a stainless steel base designed to mount directly onto the microscope sample holder. An 11 mm diameter by 4 mm deep flat bottom hole is milled into the center of the base plate to house the 4 mm tall Noliac SCMAR01 ring stack actuator. The actuator is glued to the bottom surface of the hole. The top surface of the actuator is set flush to the bottom of a 0.254 mm (0.010 in) deep counterbore that is milled into the top surface of the base plate to allow the plate flexure to rest flush with the top surface. A 0.254 mm thick circular plate flexure is glued on top of the ring actuator and into the counterbore of the base plate. The flexure plate serves to guide the actuator's vertical

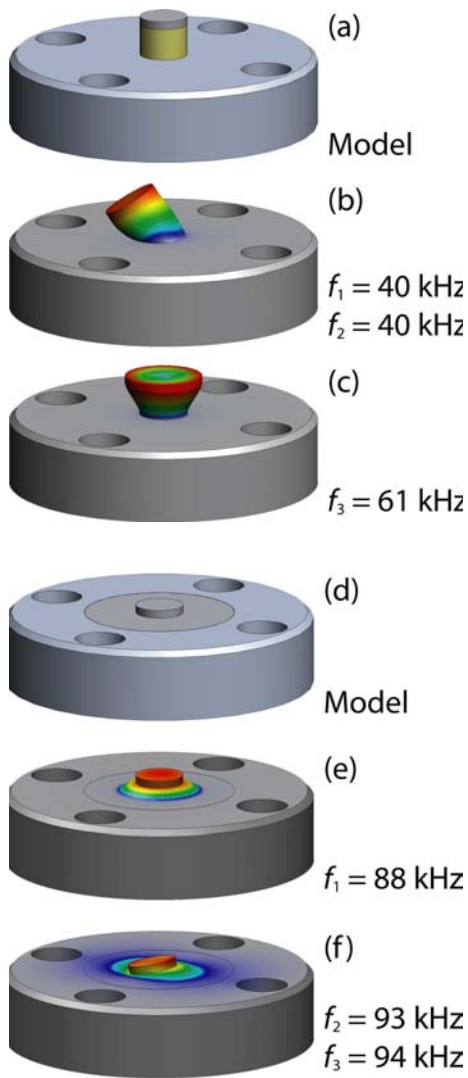


Fig. 4. Finite element analysis results for the dual-stage positioning stage: (a) the z -axis positioner with 1 mm thick steel sample platform constrained at the base; (b) first mode (bending in x/y) at 40 kHz; (c) second mode (piston) at 61 kHz; (d) base-constrained and flexure-guided (with 1 mm thick steel sample); (e) first mode (piston) at 88 kHz (44% increase); (f) second mode (bending in x/y) at 93/94 kHz respectively (133% increase).

motion and restrict unwanted out-of-axis motion, such as bending modes.

V. IMAGING EXPERIMENTS

In this section, the imaging performance of the dual-stage system is compared to the standard feedback system described in Section II. Due to a resonance at 680 Hz, the standard feedback system is limited to a gain of $\alpha=190$ which results in a closed-loop bandwidth of only 83 Hz. This is compared to a dual-stage controller with a gain of 30000.

The closed-loop frequency response, from an additive voltage at V_{ds} to the deflection dfl , is plotted in Figure 6(a). This transfer function illustrates the ability of the controller to regulate the tip-sample interaction force in the presence of disturbances introduced by the sample topography. Higher attenuation in this transfer function implies improved force

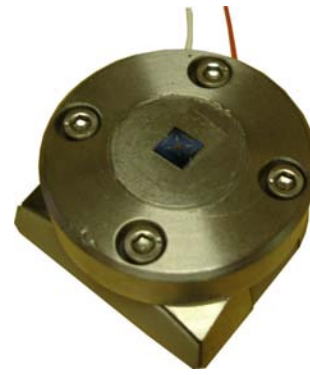


Fig. 5. Assembled high-speed vertical positioner with attached sample

regulation and higher quality imaging. Since the dual-stage controller is much higher gain, the force regulation is significantly better than the standard feedback loop.

The effect of the improved bandwidth is demonstrated in Figure 6(b) where a BudgetSensors HS-100MG calibration is imaged at 5.2 Lines/s or 520 $\mu\text{m/s}$. The lower bandwidth controller 'smears' the edges of the sample and filters small features that generate interactions above the controller bandwidth.

The cantilever deflection, which is proportional to the force error, is plotted in Figure 6(c). From this figure it can be concluded that the standard controller results in significant imaging forces applied at points where abrupt changes in the sample occur. Such forces are intolerable when imaging sensitive or soft samples that can be damaged or deformed. The dual-stage controller results in a reduction of force error from 0.810 (averaged over the whole sample) to 0.010, which is an 81 times improvement. Further proof can be observed in Figure 6(d) where a single line of the image is plotted. The low-pass characteristic of the slower controller is clearly evident.

In addition to improving the image quality, dual-stage control can also be used for increasing the imaging speed. However, with an integral controller, as speed is increased, the force error will increase proportionally. This trade-off is summarized approximately below,

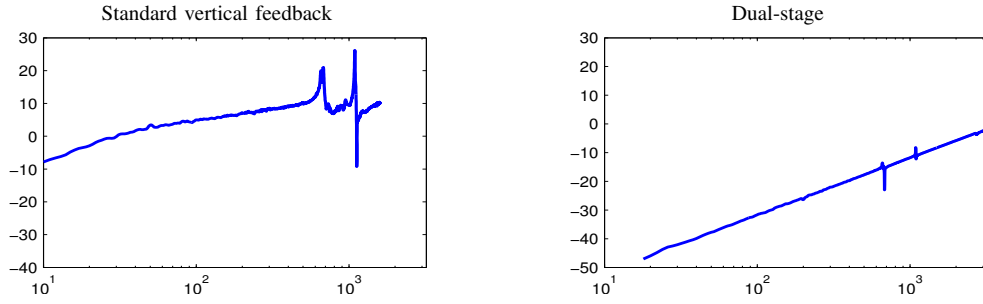
$$\text{Speed increase} \times \text{Force error reduction} = \beta. \quad (3)$$

where β is the factor by which the bandwidth is increased and the other variables are the factors by which speed and force error are reduced or increased. That is, if the imaging speed is kept constant, the dual-stage controller allows a reduction of force error by β times. Conversely, if force error is constant, the dual-stage controller allows a β times improvement in imaging speed.

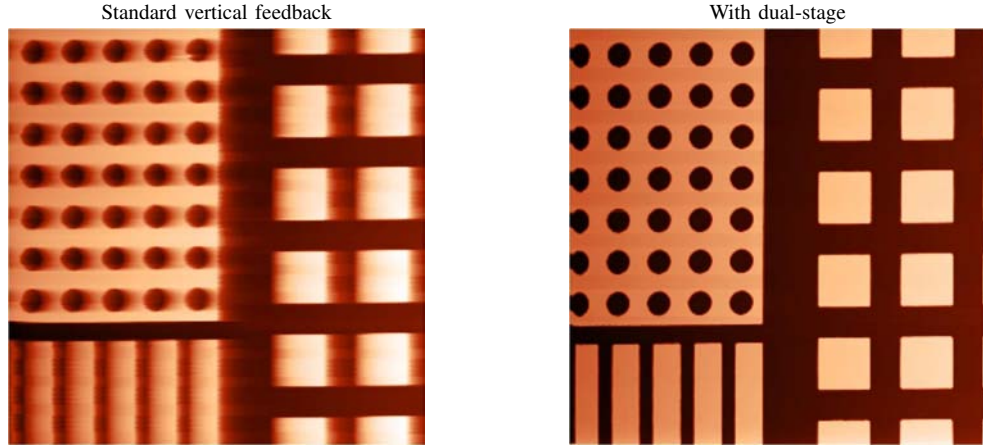
VI. CONCLUSIONS

In this work, the vertical feedback performance of an atomic force microscope is improved by adding an auxiliary high-speed vertical positioner. The high-speed positioner is used in a dual-stage configuration with the microscope's internal piezoelectric tube scanner. This results in both large

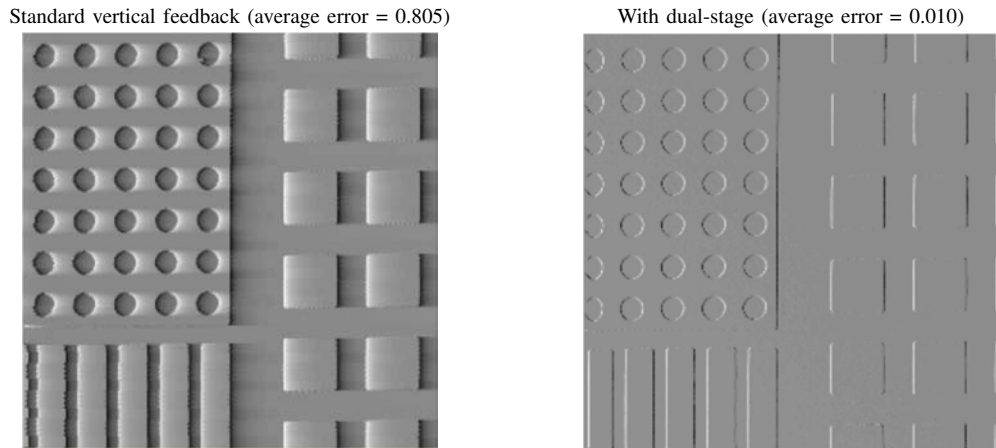
(a) Vertical feedback disturbance rejection transfer function (dB versus Hz)



(b) $50 \times 50 \mu\text{m}$ constant force images of a 100-nm feature height calibration standard, taken at $520 \mu\text{m/s}$



(c) Cantilever deflection (force error)



(d) Single image line, (vertical height in nm versus position in μm)

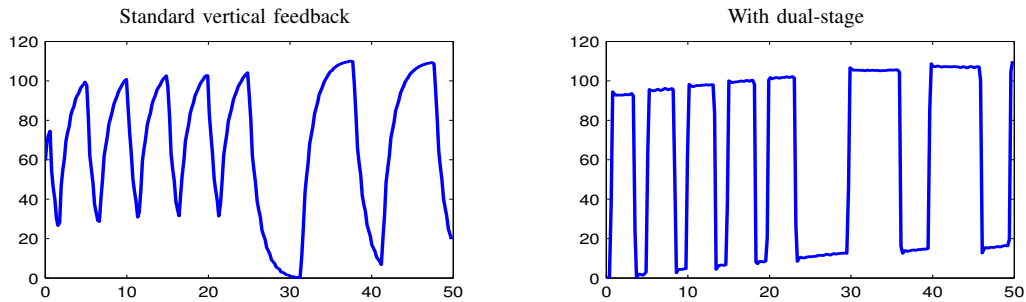


Fig. 6. Performance comparison of a standard vertical feedback controller and dual-stage controller. The images were recorded at 5.2 Hz or $520 \mu\text{m/s}$.

range and a resonance frequency improvement from 680 Hz to 88 kHz.

Finite element analysis was used to optimize the mechanical design of the high-speed positioner. A flexure was found to increase the first resonance frequency of a piezoelectric stack actuator from 44 kHz to 88 kHz. The flexure also changes the first resonance mode from an undesirable bending mode to a longitudinal mode in the same axis as the elongation.

Thanks to the increased resonance frequency, the dual-stage configuration allows an increase in the controller gain from 190 to 30000. This translates to a vast improvement in image quality or scanning speed. Visually, the dual-stage controller eliminates image smearing and faithfully reproduces fine sample features that would otherwise be lost or distorted.

Future work involves incorporating the dual-stage positioner with better lateral scanning control to achieve true constant-force contact-mode imaging at speeds approaching one-frame-per-second with a standard commercial microscope.

ACKNOWLEDGMENTS

This research was supported by the Australian Research Council (DP0666620), the Centre for Complex Dynamic Systems and Control, and in part by the Nevada NASA Space Grant Consortium. Experiments were conducted at the Laboratory for Dynamics and Control of Nanosystems, University of Newcastle. The authors also thank Tony Berendsen, Development Technician in the Mechanical Engineering Department at the University of Nevada, Reno, for his help fabricating the flexure-guided z -axis stage.

REFERENCES

- [1] G. Btrionetti, A. Bazzalia, and R. Orizio, "Atomic force microscopy: a powerful tool for surface defect and morphology inspection in semiconductor industry," *The European Physical Journal Applied Physics*, vol. 27, no. 1-3, pp. 101–106, July 2004.
- [2] A. Humphris, M. McConnell, and D. Catto, "A high-speed atomic force microscope capable of video-rate imaging," *Microscopy and Analysis - SPM Supplement*, pp. 29–31, March 2006.
- [3] J. A. Vicary and M. J. Miles, "Pushing the boundaries of local oxidation nanolithography: Short timescales and high speeds," *Ultramicroscopy*, vol. 108, no. 10, pp. 1120–1123, September 2008.
- [4] A. Ferreira and C. Mavroidis, "Virtual reality and haptics for nanorobotics," *IEEE Robotics and Automation Magazine*, vol. 13, no. 3, pp. 78–92, September 2006.
- [5] A. A. Tseng, S. Jou, A. Notargiacomo, and T. P. Chen, "Recent developments in tip-based nanofabrication and its roadmap," *Journal of Nanoscience and Nanotechnology*, vol. 8, no. 5, pp. 2167–2186, May 2008.
- [6] A. A. Tseng, Ed., *Nanofabrication: Fundamentals and Applications*. World Scientific, 2008.
- [7] M. Guthold, X. Zhu, C. Rivetti, G. Yang, N. H. Thomsson, S. Kasas, H. G. Hansma, B. Smith, P. K. Hansma, and C. Bustamante, "Direct observation of one-dimensional diffusion and transcription by *Escherichia coli* RNA polymerase," *Biophysical Journal*, vol. 77, no. 4, pp. 2284–2294, October 1999.
- [8] T. Ando, N. Kodera, T. Uchihashi, A. Miyagi, R. Nakakita, H. Yamashita, and K. Matada, "High-speed atomic force microscopy for capturing dynamic behavior of protein molecules at work," *e-Journal of Surface Science and Nanotechnology*, vol. 3, pp. 384–392, December 2005.
- [9] A. D. L. Humphris, M. J. Miles, and J. K. Hobbs, "A mechanical microscope: high-speed atomic force microscopy," *Applied Physics Letters*, vol. 86, pp. 034 106(1–3), 2005.
- [10] G. Schitter, K. J. Åström, B. E. DeMartini, P. J. Thurner, K. L. Turner, and P. K. Hansma, "Design and modeling of a high-speed AFM-scanner," *IEEE Transactions on Control Systems Technology*, vol. 15, no. 5, pp. 906–915, September 2007.
- [11] M. J. Rost, L. Crama, P. Schakel, E. van Tol, G. B. E. M. van Velzen-Williams, C. F. Overgaw, H. ter Horst, H. Dekker, B. Okhuijsen, M. Seynen, A. Vijftigschild, P. Han, A. J. Katan, K. Schoots, R. Schumm, W. van Loo, T. H. Oosterkamp, and J. W. M. Frenken, "Scanning probe microscopes go video rate and beyond," *Review of Scientific Instruments*, vol. 76, no. 5, pp. 053 710(1–9), April 2005.
- [12] L. M. Picco, L. Bozec, A. Ulcinas, D. J. Engledew, M. Antognozzi, M. Horton, and M. J. Miles, "Breaking the speed limit with atomic force microscopy," *Nanotechnology*, vol. 18, no. 4, pp. 044 030(1–4), January 2007.
- [13] A. J. Fleming, "High-speed vertical positioning for contact-mode atomic force microscopy," in *Proc. IEEE/ASME International Conference on Advanced Intelligent Mechatronics*, Singapore, July 2009, pp. 522–527.
- [14] D. Y. Abramovitch, S. B. Andersson, L. Y. Pao, and G. Schitter, "A tutorial on the mechanisms, dynamics, and control of atomic force microscopes," in *Proc. American Control Conference*, New York City, NY, July 2007, pp. 3488–3502.
- [15] S. M. Salapaka and M. V. Salapaka, "Scanning probe microscopy," *IEEE Control Systems Magazine*, vol. 28, no. 2, pp. 65–83, April 2008.
- [16] G. Schitter, "Improving the speed of AFM by mechatronic design and modern control methods," *Technisches Messen*, vol. 76, no. 5, pp. 266–273, May 2009.
- [17] T. Ando, T. Uchihashi, and T. Fukuma, "High-speed atomic force microscopy for nano-visualization of dynamic biomolecular processes," *Progress in Surface Science*, vol. 83, no. 7-9, pp. 337–437, November 2008.
- [18] T. Ando, "Control techniques in high-speed atomic force microscopy," in *Proc. American Control Conference*, Seattle, WA, June 2008, pp. 3194–3200.
- [19] K. K. Leang and A. J. Fleming, "High-speed serial-kinematic AFM scanner: design and drive considerations," *Asian Journal of Control*, vol. 11, no. 2, pp. 144–153, March 2009.
- [20] A. J. Fleming and S. O. R. Moheimani, "Sensorless vibration suppression and scan compensation for piezoelectric tube nanopositioners," *IEEE Transactions on Control Systems Technology*, vol. 14, no. 1, pp. 33–44, January 2006.
- [21] A. J. Fleming and K. K. Leang, "Charge drives for scanning probe microscope positioning stages," *Ultramicroscopy*, vol. 108, no. 12, pp. 1551–1557, November 2008.
- [22] S. Devasia, E. Eleftheriou, and S. O. R. Moheimani, "A survey of control issues in nanopositioning," *IEEE Transactions on Control Systems Technology*, vol. 15, no. 5, pp. 802–823, September 2007.
- [23] A. J. Fleming and A. G. Wills, "Optimal periodic trajectories for band-limited systems," *IEEE Transactions on Control Systems Technology*, vol. 13, no. 3, pp. 552–562, May 2009.
- [24] S. O. R. Moheimani, "Accurate and fast nanopositioning with piezoelectric tube scanners: Emerging trends and future challenges," *Review of Scientific Instruments*, vol. 79, no. 7, pp. 071 101(1–11), July 2008.
- [25] T. Sulchek, S. C. Minne, J. D. Adams, D. A. Fletcher, A. Atalar, C. F. Quate, and D. M. Adderton, "Dual integrated actuators for extended range high speed atomic force microscopy," *Applied Physics Letters*, vol. 75, no. 11, pp. 1637–1639, 1999.
- [26] Y. Jeong, G. R. Jayanth, and C.-H. Menq, "Control of tip-to-sample distance in atomic force microscopy: A dual-actuator tip-motion control scheme," *Review of Scientific Instruments*, vol. 78, no. 9, pp. 093 706(1–7), 2007.
- [27] T. Akiyama, U. Staufer, and N. F. de Rooij, "Atomic force microscopy using an integrated comb-shape electrostatic actuator for high-speed feedback motion," *Applied Physics Letters*, vol. 76, no. 21, pp. 3139–3141, May 2000.
- [28] G. Schitter, W. F. Rijkée, and N. Phan, "Dual actuation for high-bandwidth nanopositioning," in *Proc. IEEE Conference on Decision and Control*, Cancun, Mexico, December 2008, pp. 5176–5181.
- [29] Y. Yan, Y. Wu, Q. Zou, and C. Su, "An integrated approach to piezo-actuator positioning in high-speed atomic force microscope imaging," *Review of Scientific Instruments*, vol. 79, pp. 073 704(1–9), July 2008.
- [30] J. Maess, A. J. Fleming, and F. Allgöwer, "Simulation of dynamics-coupling in piezoelectric tube scanners by reduced order finite element models," *Review of Scientific Instruments*, vol. 79, pp. 015 105(1–9), January 2008.